Sensitivity of Retrieved Aerosol Properties to Assumptions in the Inversion of Spectral Optical Depths

HELENA GONZÁLEZ JORGE

Departamento de Física Fundamental y Experimental, Universidad de La Laguna, La Laguna, Spain, and Climate Monitoring and Diagnostic Laboratory, National Oceanic and Atmospheric Administration, Boulder, Colorado

JOHN A. OGREN

Climate Monitoring and Diagnostic Laboratory, National Oceanic and Atmospheric Administration, Boulder, Colorado

(Manuscript received 27 December 1994, in final form 27 March 1996)

ABSTRACT

The uncertainties of integral aerosol properties calculated using aerosol size distributions retrieved from multiwavelength observations of aerosol optical depth have been determined for a variety of typical atmospheric aerosol size distributions and refractive indices. The results suggest that more information about the aerosol composition, as well as more information about the sizes that are less efficient, in the optical sense, is needed to improve the shape of the retrieved size distributions. All the calculations in this paper assume spherical homogeneous particles. The sensitivity results refer to these conditions. The moments of the retrieved size distributions are systematically underestimated and errors can be as large as −82%, −30%, and −35% for the total number of particles, the total surface, and the total volume, respectively. The errors in the mass scattering efficiency, the effective radius, and the total volume depend very much on whether the actual volume size distribution is monomodal or bimodal. For a known refractive index, the total scattering coefficient, the hemispherical backscattering coefficient, and the extinction coefficient, as well as the hemispheric backscattering to total scattering ratio and the asymmetry factor, are obtained with absolute values for the average errors less than 4%. Similar behavior was expected for cases with uncertainty in the refractive index, especially for parameters defined by the ratio of two integral properties. However, it turns out that the hemispheric backscattering coefficient and the hemispheric backscattering to total scattering ratio were poorly retrieved, reaching errors of 29% in several cases, while the asymmetry factor was very well recovered with absolute values of the average errors always under 7%. When the wavelength dependence of the refractive index is included, the retrieved size distribution is very unrealistic, with average errors in the hemispheric backscattering coefficients and the hemispheric backscattering to total scattering ratio around 30% at some wavelengths. However, even in this case the errors in the retrieved asymmetry factor stay under 8%. Thus, for spherical and homogeneous particles, the spectral optical depth data can be used to determine the asymmetry factor with little sensitivity to the assumptions in the calculations. Furthermore, the retrieved size distribution can be used as an intermediate step to extrapolate one set of optical properties from another set of optical properties.

1. Introduction

Tropospheric aerosols contribute to global climate change by scattering and absorption of sunlight at visible wavelengths. The sign of this aerosol forcing depends on the amount of energy that returns to space (cooling effect) versus the amount of energy that is trapped in the lower atmosphere due to absorption (warming effect). The final magnitude of the direct local aerosol forcing must be added or subtracted to the forcing by greenhouse gases and to the indirect aerosol forcing (aerosol forcing of climate through cloud modification). Several efforts have been made to estimate the aerosol perturbation of the earth radiation budget (e.g., Charlson et al. 1991; Hansen and Lacis 1990; Charlson et al. 1992; Kiehl and Briegleb 1993; Schneider 1994; Taylor and Penner 1994). Their calculations are based on estimates of the aerosol integral optical properties in the visible range, which can be made directly from observed parameters or obtained from assumptions of the aerosol compositions and size distributions.

The size distributions can be measured directly in situ or retrieved from indirect information of the aerosols, which is associated with the wavelength dependence of one or more optical properties or/and with the angular dependence. In this regard, many inversion al-

Corresponding author address: Dr. Helena González Jorge, Departamento de Fisica Fundamental y Experimental, Universidad de La Laguna, Avda. Astrofisico Francisco Sánchez, 38204 La Laguna, Tenerife, Spain.
E-mail: johno@cmdl.noaa.gov

gorithms have been developed in the last decades covering a wide range of possibilities, from using one type of integral optical property to using aerosol property combinations such as scattered radiances with optical depths, extinction coefficients with scattering phase functions, etc. (Yamamoto and Tanaka 1969; Grassl 1971; Heintzenberg 1975, 1980; King et al. 1978; Shaw 1979; Nakajima et al. 1983; Dellago and Horvarth 1993). They all seek the solution of a system of integral equations that can be solved by several mathematical algorithms. Since there is no unique solution, they all require a step to determine which results better represent the actual size distribution in the atmosphere. Further, the retrievals must account for all the other aerosol properties.

This study deals only with the inversion of optical thickness, and its aim is to determine which aerosol properties are least sensitive to the assumptions in the inversion algorithm and to determine which properties are the least variable for the many retrieved size distributions that satisfy the initial spectral optical depths. Multiwavelength optical depths have been measured for a long time and for many different locations and may provide useful information about other aerosol parameters. To accomplish this, we use the inversion algorithm of King et al. (1978).

2. Procedure

a. The inversion algorithm

The integral equation to be solved is (King et al. 1978)

$$\tau(\lambda, m^*) = \int_0^\infty \int_0^\infty \pi r^2 Q_e(r, \lambda, m^*) n(r, z) dz dr, \quad (1)$$

where $\tau(\lambda, m^*)$ is the measured optical depth; $n(r, z)$ is the number size distribution, that is, the number of particles with radii between r and $r + dr$ at the atmospheric height z; $Q_e(r, \lambda, m^*)$ is the extinction efficiency factor; m^* is the aerosol complex refractive index; and λ is the wavelength of the incident light. For simplicity, m^* is considered to be independent of λ and z. The assumption of an homogeneous aerosol column in the atmosphere allows the integration over height and then Eq. (1) is rewritten as

$$\tau(\lambda, m) = \int_0^\infty \pi r^2 Q_e(r, \lambda, m) n_c(r) dr, \quad (2)$$

where $n_c(r)$ is the columnar aerosol number size distribution and m is an effective refractive index that represents the average composition of the aerosol particles. Equation (2) is solved by an iterative method described by King et al. (1978). They write $n_c(r) = f(r)h(r)$, where $h(r) = r^{-(\upsilon+1)}$ is the Junge power law and $f(r)$ is the unknown part of the column size distribution. With this substitution, they apply a quadrature method and a minimization procedure leading to the solution vector

$$f = (\mathbf{A}^T\mathbf{C}^{-1}\mathbf{A} + \gamma\mathbf{H})^{-1}\mathbf{A}^T\mathbf{C}^{-1}\tau, \quad (3)$$

where $\mathbf{C}$ is the measurement covariance matrix; γ is a nonnegative Lagrange multiplier; $\mathbf{H}$ is a smoothing matrix; $\mathbf{A}$ is the matrix representation of the kernel functions. In the first iteration, the elements of $\mathbf{A}$ ($A_{ij}^{(1)} = A_{ij}^{(1)}(\lambda_i, r_j)$) are given by

$$A_{ij}^{(1)} = \int_{r_j}^{r_{j+1}} \pi r^2 Q_e(r, \lambda_i, m) r^{-(\nu+1)} dr, \quad (4)$$

and $f^{(1)}(r_{m_j})$ (with r_{m_j} the midvalue of r in the interval $[r_j, r_{j+1}]$) is obtained with the substitution of $\mathbf{A}^{(1)}$ in (3). In the second iteration, the elements of $\mathbf{A}^{(2)}$ become

$$A_{ij}^{(2)} = f^{(1)}(r_{m_j}) \int_{r_j}^{r_{j+1}} \pi r^2 Q_e(r, \lambda_i, m) r^{-(\nu+1)} dr, \quad (5)$$

and $f^{(2)}(r_{m_j})$ will be obtained through (3). The iterative procedure continues until a stable solution is reached. Since the shape of the number size distribution is being assumed partially in the inversion with the power law [Eq. (4)], the number of inverted sizes can exceed the number of measured optical depths.

The exponents ν are calculated by applying the empirical formula of Ångström:

$$\tau(\lambda, m) = \beta\lambda^{-\mathring{a}}, \quad (6)$$

where $\mathring{a} = \nu - 2$ is calculated by linear least-squares methods as a first guess. The program is considered to work properly when the inversion of the optical depths using the three guesses $\nu - 1$, ν, $\nu + 1$ yields the same results (King et al. 1978). In this case, it is considered that the retrievals are independent of the initial value of ν.

b. Sources of uncertainty in the inversion of spectral optical depths

1) NUMERICAL ERRORS

The loss of accuracy in going from an integral to a finite sum is rarely the main difficulty encountered in inversion problems (Twomey 1977; King 1982). However, if the finite sum of the quadrature method has few terms, say five, the calculated optical depths integrating over the retrieved size distribution are inconsistent with their initial values. Even though the inversion program calculates good estimates of the input data in the minimization step of the algorithm, the optical depths calculated over the retrievals are overestimated. Increasing the number of radii to 15 yields a good agreement between the initial and retrieved optical depths.

2) ASSUMPTIONS OF MIE THEORY

All Mie calculations assume that the particles are spherical in shape. The effects of nonspherical particles

on the inversion of nephelometer results have been studied by Heintzenberg (1978), who concluded that applying Mie theory to nonspherical particles systematically distorts the derived size distribution, leading to a shift in the concentration maximum to smaller sizes and increasing the number concentrations by sometimes more than a factor of 10. Even though this is a problem when analyzing real data, we will not evaluate here its consequences, and we will assume spherical and homogeneous particles for all the calculations.

3) INTERDEPENDENCE OF THE INFORMATION CONTENT IN THE SPECTRAL OPTICAL DEPTH AND THE SENSITIVITY TO THE FINITE RADIUS INTERVAL

It is important to choose an appropriate radius interval to perform the inversion. The cutoff sizes must be selected according to the extinction efficiency factor at the given wavelengths. For visible light, particles with radius less than 0.05 μm do not contribute much to the extinction coefficient because the extinction efficiency factor is very close to zero. Also for visible light, the extinction efficiency factors of particles with radius larger than 2 μm converge to a constant value of 2 and have very little dependence on the wavelengths. Therefore, the largest radius interval should be from 0.05 to 2 μm. On the other hand, atmospheric aerosol size distributions can be characterized by a multimodal model consisting of additive lognormal distributions (Whitby 1978). The observed parameters vary depending on the aerosol sources and locations, and the accumulation and coarse modes are defined by lognormal distributions with geometric volume mean radii from 0.075 to 0.25 μm and from 2.5 to 15 μm, respectively (Whitby 1978). Then these two modes can be retrieved (partially) from spectral optical depths at visible wavelengths.

Another requirement for choosing the appropriate radius interval is that the optical coefficients, that is, the total scattering coefficient, the hemispherical backscattering coefficient, and the extinction coefficient, should contain independent information about the particles. Heintzenberg et al. (1981) developed a criterion. They represented the ratios of kernel functions at different wavelengths, $K_{\text{ext}}(r, \lambda_i, m) = 3Q_e(r, \lambda_i, m)/4r$, as a function of the particle radius, and then selected the interval of radius where the ratios are not constant. We will use this criterion to select the initial radius interval, which is an input parameter that can be changed by the algorithm, meaning that the final retrievals can be over different size intervals. We will study both the full size distribution, where we consider an infinite radius interval, and the truncated size distribution, where we only consider the radius interval of the retrieval.

4) SENSITIVITY TO THE COMPOSITION OF THE AEROSOL PARTICLES

Two different chemical species can have the same size distribution. Since the optical properties depend strongly on the refractive index of the aerosols, the assumption of a wrong refractive index in the inversion will lead to an incorrect size distribution. Moreover, the aerosol composition through the atmospheric column varies and the refractive index must be considered as a function of height. Hence, retrieving the size distribution assuming a unique refractive index in the column disregards the whole dependence of the measured optical depths on the composition. Besides, the refractive index of each chemical species depends also on wavelength.

We will address in this paper the effects of points 2b(3) and 2b(4).

c. Integral aerosol properties

The total number of particles (N), the total surface (S), and the total volume (V) in a unit volume of air are useful integral properties for characterizing the size distribution. The effective radius, r_{eff}, is the relationship between two moments of the size distribution, the total volume, and the total surface:

$$r_{\text{eff}} = \frac{\int_0^\infty r^3 n(r)\,dr}{\int_0^\infty r^2 n(r)\,dr} = \frac{3V}{S}. \tag{7}$$

Here r_{eff} is very sensitive to changes in the relative amount of particles of different sizes. The optical coefficients that contain independent information about particle sizes for a real refractive index are the scattering $[\sigma_{\text{sp}}(\lambda, m)]$ and hemispheric backscattering $[\sigma_{\text{bsp}}(\lambda, m)]$ coefficients. When the refractive index is complex, the extinction $[\sigma_e(\lambda, m)]$ or the absorption coefficients $[\sigma_{\text{ap}}(\lambda, m)]$ must be included. As the aerosol layer has been assumed homogeneous, the optical depth $[\tau(\lambda, m)]$ is just the column height (z) times the extinction coefficient. The mass scattering efficiency is an example of the magnitudes relating the optical properties and the moments of the size distribution. It is defined by

$$\alpha_{\text{sp}}(\lambda, m) = \sigma_{\text{sp}}(\lambda, m)/M, \tag{8}$$

and the total mass, M, is calculated for the total volume of the retrievals assuming a constant density equal to 1.77 for the aerosol particles.

The asymmetry factor expresses the amount of energy scattered in the backward versus forward directions. For a particle of radius r, the asymmetry factor may be defined by

$$g(r, \lambda, m) = \frac{\left[\int_0^\pi \beta(\theta, r, \lambda, m)\sin(\theta)\cos(\theta)\,d\theta\right]}{\left[\int_0^\pi \beta(\theta, r, \lambda, m)\sin(\theta)\,d\theta\right]}, \tag{9}$$

where λ is the wavelength of the incident light, m is the refractive index, and $\beta(\theta, r, \lambda, m)$ is the angular scattering phase function, that is, the intensity of radiation scattered in the direction given by the scattering angle θ. The angular scattering phase function may be written using Mie theory as

$$\beta(\theta, r, \lambda, m) = (\lambda^2/8\pi^2)[i_1(\theta, r, \lambda, m) + i_2(\theta, r, \lambda, m)], \quad (10)$$

where $i_1(\theta, r, \lambda, m)$ and $i_2(\theta, r, \lambda, m)$ are the intensity functions with polarization perpendicular and parallel to the scattering plane, respectively. For a size distribution of particles,

$$\beta'(\theta, \lambda, m) = \int_0^\infty n(r)\beta(\theta, r, \lambda, m)dr, \quad (11)$$

and the asymmetry factor becomes

$$g(\lambda, m) = \frac{\left[\int_0^\pi \beta'(\theta, \lambda, m) \sin(\theta) \cos(\theta)d\theta\right]}{\left[\int_0^\pi \beta'(\theta, \lambda, m) \sin(\theta)d\theta\right]}. \quad (12)$$

Let (11) be substituted in (12), interchange the order of integration and make use of (9). This yields in the numerator of (12)

$$\int_0^\infty n(r)g(r, \lambda, m)\left(\int_0^\pi \beta(\theta, r, \lambda, m) \sin(\theta)d\theta\right)dr \quad (13)$$

and in the denominator

$$\int_0^\infty n(r)\left[\int_0^\pi \beta(\theta, r, \lambda, m) \sin(\theta)d\theta\right]dr. \quad (14)$$

Defining the scattering efficiency factors by

$$Q_{sp}(r, \lambda, m) = (1/2r^2)\int_0^\pi \beta(\theta, r, \lambda, m) \sin(\theta)d\theta, \quad (15)$$

and substituting (15) into (13) and (14), (12) leads to

$$g(\lambda, m) = \frac{\int_0^\infty r^2n(r)g(r, \lambda, m)Q_{sp}(r, \lambda, m)dr}{\int_0^\infty r^2n(r)Q_{sp}(r, \lambda, m)dr}. \quad (16)$$

The hemispheric backscattering to total scattering ratio expresses the fraction of energy that is scattered in the backward direction and is defined for a particle of radius r by

$$R(r, \lambda, m) = \frac{\int_{\pi/2}^\pi \beta(\theta, r, \lambda, m) \sin(\theta)d\theta}{\int_0^\pi \beta(\theta, r, \lambda, m) \sin(\theta)d\theta}. \quad (17)$$

Following the previous steps used for the asymmetry factor, the hemispheric backscattering to total scattering ratio for a size distribution of particles, $R(\lambda, m)$, may be rewritten as

$$R(\lambda, m) = \frac{\int_0^\infty r^2n(r)R(r, \lambda, m)Q_{sp}(r, \lambda, m)dr}{\int_0^\infty r^2n(r)Q_{sp}(r, \lambda, m)dr}, \quad (18)$$

where $R(r, \lambda, m)Q_{sp}(r, \lambda, m) = Q_{bsp}(r, \lambda, m)$, the hemispheric backscattering efficiency. The functions $g(r, \lambda, m)Q_{sp}(r, \lambda, m)$, $Q_{sp}(r, \lambda, m)$, and $Q_{bsp}(r, \lambda, m)$ are shown in Fig. 1. Note that $g(r, \lambda, m)Q_{sp}(r, \lambda, m)$ is in phase with $Q_{sp}(r, \lambda, m)$ and altering the concentrations or the sizes of the particles yields similar effect on both integrals of (16). However, $Q_{bsp}(r, \lambda, m)$ is not in phase with $Q_{sp}(r, \lambda, m)$, and, depending on their sizes, the aerosol particles may have opposite effects on the numerator and the denominator of (18). Therefore, any distortion of the retrieved size distribution leads to larger errors in the hemispheric backscattering to total scattering ratio than in the asymmetry factor.

3. Tests and results

Calculation of the optical efficiency factors is described in Wiscombe (1980). To simulate the size distribution, each mode was implemented using a lognormal size distribution (Table 1) based on the average size distributions of Whitby (1978); both monomodal

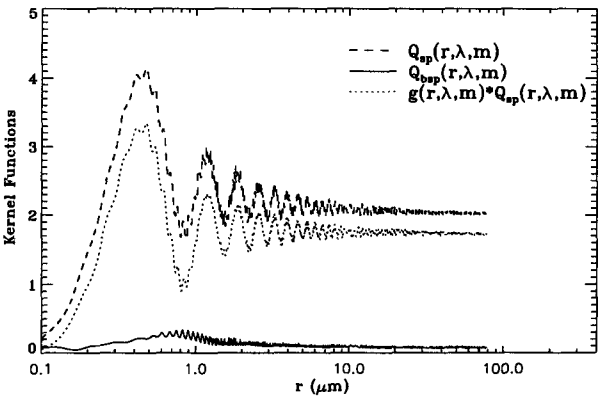

FIG. 1. Particle radius dependence of the kernel functions that differentiate the asymmetry factor from the backscattering to total scattering ratio (m = 1.50, λ = 0.62 μm).

TABLE 1. Parameters of the number size distributions used to generate the optical depths needed in the inversion procedure.

	Monomodal			Bimodal[a]						
Size distribution[b]	A	B	C	D	E	F	G	H	I	J
Total number (cm^{-3})	13000	2300	32000	13000 4.2	13000 2.0	6500 4.2	13000 0.42	13000 42.0	13000 4.2	13000 4.2
Mean radius (μm)	0.0345	0.038	0.027	0.0345 0.485	0.0345 0.485	0.0345 0.485	0.0345 0.485	0.0345 0.485	0.0518 0.485	0.0173 0.485
Geometric standard deviation	2.03	2.00	2.16	2.03 2.15	2.03 2.15	2.03 2.15	2.03 2.15	2.03 2.15	2.03 2.15	2.03 2.15

[a] The upper values correspond to the accumulation modes and the lower values to the coarse modes.

[b] A, B, and C are the accumulation modes of the average continental, average background, and average urban size distributions, respectively (Whitby 1978). D is the average accumulation + coarse modes of the average continental size distribution (Whitby 1978). E, F, G, and H combine two modes of clearly different volumes to compare the effects of the relative concentrations of the accumulation and coarse mode. I and J are like D except for the accumulation mode that is shifted 50% to larger and smaller radius, respectively.

and bimodal distributions are included to allow the study of fine and coarse particles independently and combined. The refractive indices used are $1.40-0.0i$, $1.45-0.0i$, $1.50-0.0i$, $1.45-0.001i$, and $1.45-0.01i$. The real parts have been selected between 1.33 (pure water) and 1.54 (silicates) as in King et al. (1978). The imaginary parts cover a range from nonabsorbing to moderately absorbing particles. These refractive indices are representative of many tropospheric aerosols (Tang and Munkelwitz 1994; Palmer and Williams 1975; Toon et al. 1976). Results of this sensitivity study may be extrapolated for other refractive indices in the interval of real parts (1.35, 1.55). Except in the case where a different set of wavelengths is specified, we used a set of seven wavelengths equally spaced from 0.35 to 0.88 μm (0.35, 0.44, 0.53, 0.62, 0.70, 0.79, 0.88 μm).

Following the criteria of Heintzenberg et al. (1981), the independent aerosol information content in the optical depths was in the radius interval 0.06 to 2 μm. We used this starting interval for all our calculations. However, when the refractive index was real, the radius range could be extended to 4–5 μm. Conversely, when the particles were allowed to absorb radiation, the kernel functions were quite smoothed, and the radius range was more restricted. The number of inverted sizes was always 15 [see sections 2a and 2b(1)].

a. Uncertainties in retrievals with known refractive index

The general procedure consisted of the following steps.

1) Consider a size distribution $n(r)$ (Table 1) and the index of refraction m.

2) Calculate $\tau(\lambda, m)$, $\sigma_{sp}(\lambda, m)$, $\sigma_{bsp}(\lambda, m)$, $\sigma_e(\lambda, m)$, N, S, V, r_{eff}, $R(\lambda, m)$, $g(\lambda, m)$, $\alpha_{sp}(\lambda, m)$ for the size distribution $n(r)$.

3) Use the inversion algorithm to infer the size distributions $n'(r)$ from $\tau(\lambda, m)$ assuming the same refractive index m. Note that the inversion algorithm calculates many size distributions that satisfy the given $\tau(\lambda, m)$.

4) Calculate $\sigma'_{sp}(\lambda, m)$, $\sigma'_{bsp}(\lambda, m)$, $\sigma'_e(\lambda, m)$, N', S', V', r'_{eff}, $R'(\lambda, m)$, $g'(\lambda, m)$, $\alpha'_{sp}(\lambda, m)$ for the retrievals, $n'(r)$. Each parameter has a mean value and standard deviation for the set of solutions in (3).

5) Calculate $\sigma''_{sp}(\lambda, m)$, $\sigma''_{bsp}(\lambda, m)$, $\sigma''_e(\lambda, m)$, N'', S'', V'', r''_{eff}, $R''(\lambda, m)$, $g''(\lambda, m)$, $\alpha''_{sp}(\lambda, m)$ for the truncated size distributions, $n''(r)$, that is, $n(r)$ only considered in the radius interval of $n'(r)$.

6) Compare (2) and (4), and compare (2) and (5).

7) Repeat for many different $n(r)$ and m.

The results of the inversion were always insensitive to the initial estimate of the slope of the power-law distribution and the retrievals, after eight iterations, converged for the three starting guesses of υ [see sections 2a and 2b(1)]. The true and the retrieved optical depths differed by less than 1%. Figure 2a illustrates both the true and retrieved number size distributions. Clearly, the retrieved size range needs to extend to smaller sizes to obtain the true shape of the number size distribution. However, there is no information of the smaller sizes in the spectral optical depths, so complementary information about these particles is needed to reproduce this part of the size distribution. We attempted the same inversion but extended to shorter radius, going from 0.006 to 2 μm instead of going from 0.06 to 2 μm. Figure 2b shows that the smallest retrieved radius was 0.03 μm and that even though the input radius interval was broad enough to cover the full size distribution, the true shape was not recovered.

When the spectral optical depths were computed for the bimodal size distributions of Table 1, the retrieved volume size distribution tended to be always bimodal except for G, J. However, the shape of the coarse mode was poorly reproduced, the minimum between the two modes was shifted by about 0.3 μm to a smaller radius, and the retrieved volume at this radius was approximately 20%–40% larger than the true value. We have

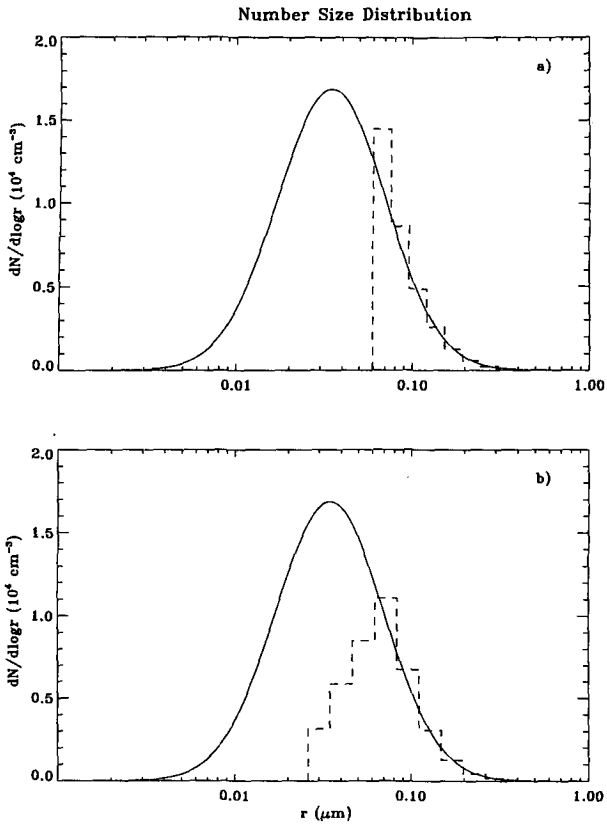

FIG. 2. Retrieved number size distributions (histograms) for two different starting radius intervals: (a) 0.06–2 μm and (b) 0.006–2 μm. The optical depth data have been generated for the monomodal size distribution A (solid line, see Table 1) using a real refractive index of 1.40. The same refractive index has been assumed in the inversion program.

found that the coarse volume size distribution was somewhat better recovered for cases where the volume of the true coarse mode exceeds the volume of the true accumulation mode. For a better estimation of the coarse mode, Dellago and Horvarth (1993) suggested to extend the interval of wavelengths farther in the infrared part of the spectrum.

Table 2 shows the mean errors and the standard deviations for the calculated parameters. The errors in the retrieved and truncated size distributions are compared to evaluate what is the effect of the retrieved radius range. The statistics were performed for the five assumed refractive indices, including all the solutions of the inversion, that is, the results for the three different initial guesses of ν and the results for the different cutoff radius. (Remember that the inversion program was able to change the selected radius interval several times.) The average errors of the moments of the retrievals were systematically smaller than the average errors of the truncated size distribution. This decrease in the average errors was because the algorithm set a larger number of particles in the retrievals to compensate for the contribution to the extinction of the excluded particles when the radius interval was made finite. The errors in the effective radius had a very different behavior depending on whether a monomodal or a bimodal size distribution was used. The smaller particles ($r < 0.06$ μm), which were always excluded from the retrievals, contribute less to the total volume than to the total surface. Thus, for monomodal true size distributions, S' was worse retrieved than V' and r'_{eff} was overestimated. For true bimodal size distributions both the smaller ($r < 0.06$ μm) and larger ($r > 2$ μm) particles were excluded; therefore, the balance between V' and S' was almost not altered. However, since these larger sizes are quite efficient light scatterers, some extra particles were placed between the two modes to compensate for their loss. This led to overestimated or underestimated r'_{eff}, depending on the relative concentrations of the excluded and extra particles.

The average errors for the retrieved scattering and extinction coefficients were less than 1% with standard deviations around 1%. However, the shapes of the retrieved scattering or extinction size distributions differed from the true shapes, especially for longer wavelengths (Fig. 3). The hemispheric backscattering coefficient was the retrieved component that most depended on the particular solution of the inversion with a strong wavelength dependence. The errors in the hemispheric backscattering to total scattering ratio were related to the errors in the hemispheric backscattering coefficient and had the same dependencies on wavelength. The asymmetry factor was the most stable retrieved parameter. Only the retrieved scattering and extinction coefficients had smaller standard deviations than g. Finally, the mass scattering efficiency was one of the worst recovered integral properties and was always systematically overestimated as a consequence of the errors in the retrieved total volume. Similar behavior is expected for any parameter obtained by dividing a well-retrieved optical property by a moment of the size distribution.

We used input data at seven wavelengths for the preceding calculations. However, it is interesting to know whether this set of optical depths contains redundant information to retrieve the size distribution. Therefore, we explored the effects of using only three or five optical depths at equally spaced wavelengths. For the monomodal distributions (A, B, and C in Table 1), seven, five, and three measured wavelengths yielded the same monomodal shapes. For bimodal distributions, the number of wavelengths needed to retrieved bimodal shapes depended on the relative concentrations of the accumulation and the coarse modes. Except for the distributions G and J in Table 1, five and seven wavelengths both yielded bimodal distributions with large errors in the vol-

TABLE 2. Average errors and standard deviations of the errors in the calculated parameters. The refractive index stays constant throughout the process. The statistics include all the solutions of the inversion of the optical depths generated for the size distributions of Table 1.

	Retrieved parameters		True truncated parameters		Retrieved parameters		True truncated parameters	
	Average error[b] (%)[a]	Standard deviation[c]	Average error (%)	Standard deviation	Average error (%)	Standard deviation	Average error (%)	Standard deviation
Total number	−82	6	−84	6	−82	11	−84	11
Total surface	−28	7	−35	9	−30	15	−36	16
Total volume	−8	3	−14	6	−35	18	−34	15
Effective radius	27	4	31	4	2	57	8	30
Extinction coefficient	0.6	0.8	−1.8	2	0.0	1.2	−9.3	8.3
Total scattering coefficient	0.7	0.8	−1.6	2	0.8	2.3	−8.7	8.0
Hemispheric backscattering coefficient	−0.8	5	−6.5	7	3.5	8.2	−9	8.2
Hemispheric backscattering to total scattering ratio	−1.5	5	−5	5	2.6	7.1	−0.1	6.2
Asymmetry factor	0.1	1	1	1	−1.4	1.9	−0.6	1.7
Mass scattering efficiency	10	4	14	7	69	51	44	27
	Monomodal size distributions (Number of retrievals = 777)				Bimodal size distributions (Number of retrievals = 645)			

[a] Error (%) = [(known value − calculated value)/known value]100.

[b] Average error (%) = $(1/N_t)\ \Sigma_i\ (\text{Error})_i$.

[c] Standard deviation = $(1/N_t)\ \langle \Sigma_i \{[(\text{error})_i - \text{average error}]/(\text{error})_i\}^2 \rangle^{1/2}$ N_t is the total number of data in the statistics and is equal to the number of retrieved size distributions for the moments and the effective radius and equal to the number of retrievals times 7 for the other parameters.

ume of the coarse mode. Size distributions inferred from three optical depths changed gradually from monomodal to bimodal shape as the relative volumes of the accumulation and coarse mode changed (Figs. 4a, 4b, and 4c). Bimodal distributions were retrieved only when the coarse volume was clearly larger than the accumulation volume. This can be interpreted by looking at the wavelength dependence of the optical depths, which is very strong for the accumulation mode and very weak for the coarse mode. The inversion program retrieves first the best accumulation mode satisfying this wavelength dependence. If its contribution is not enough to reproduce the optical depths, the particles of the coarse mode are included. Figure 4d emphasizes this point in a different way. For those solutions where the retrieved radius range was shifted to higher values, the accumulation mode had fewer particles and was unable to reproduce the measurements by itself. In these cases, the coarse mode appeared even when its volume was smaller than the volume of the accumulation mode. Since the distributions G and J are characterized for huge accumulation and insignificant coarse volumes, more than seven wavelengths are needed to retrieve some coarse particles.

The average errors of all the retrieved parameters were not affected when using five instead of seven input data. When using three wavelengths, the errors were never larger than 10% and showed a strong dependency on the refractive index.

b. *Effects of uncertainties in the refractive index*

1) PROPAGATION OF THE UNCERTAINTY IN THE ASSUMED CONSTANT REFRACTIVE INDEX

The inversion algorithm uses a single refractive index, while the true refractive index varies with particle composition and concentration, that is, with height. This fact has been treated by Yamamoto and Tanaka (1969) and by King et al. (1978). They showed that the shape of the retrieved aerosol size distribution was not substantially altered under various assumptions of refractive indices. To study how a wrong assumption of the refractive index affects the errors in the retrieved parameters, we repeated the above tests but used a different refractive index for the retrievals than was used to calculate the true optical depths:

1) Let the size distribution be $n(r)$ and the index of refraction m. (Bimodal distributions are the most frequently found in the atmosphere.)

2) Calculate $\tau(\lambda, m)$, $\sigma_{sp}(\lambda, m)$, $\sigma_{bsp}(\lambda, m)$, $\sigma_e(\lambda, m)$, $N, S, V, r_{eff}, R(\lambda, m)$, $g(\lambda, m)$, $\alpha_{sp}(\lambda, m)$ for $n(r)$.

3) Infer the size distribution $n'(r)$ from $\tau(\lambda, m)$ assuming a different index of refraction m'.

4) Calculate $\sigma'_{sp}(\lambda, m')$, $\sigma'_{bsp}(\lambda, m')$, $\sigma'_e(\lambda, m')$, $N', S', V', r'_{eff}, R'(\lambda, m')$, $g'(\lambda, m')$, $\alpha'_{sp}(\lambda, m')$ for the retrievals $n'(r)$.

5) Compare 2) and 4).

6) Repeat steps 3), 4), and 5) for many different m'.

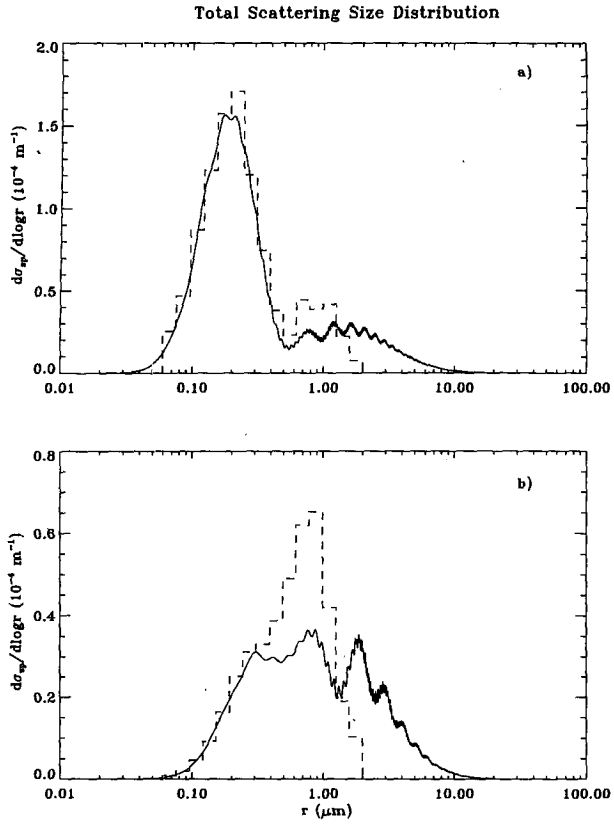

FIG. 3. Retrieved scattering size distributions (histograms) at (a) 0.35 μm and (b) 0.88 μm. The optical depth data have been generated for the bimodal size distribution F (solid line, see Table 1) using a real refractive index of 1.40. The same refractive index was assumed in the inversion program. The retrieved accumulation mode light scattering is well reproduced at 0.35-μm wavelength. However, there is an excess of retrieved particles larger than 0.3 μm to compensate for the contribution of the unretrieved particles larger than 2 μm. This excess of particles greatly distorts the light scattering size distribution at longer wavelengths.

7) Repeat for many different $n(r)$ and m.

The sensitivity of the inverted size distributions to the refractive index agreed with the results of Yamamoto and Tanaka (1969) and King et al. (1978). Besides, the retrievals were consistent with the optical depth dependencies on the refractive indices stated by Grassl (1971). They were more sensitive to the uncertainties in the real part of the refractive index (Fig. 5a) than to the uncertainties in the imaginary part (Fig. 5b). For the retrieved moments of the size distribution, the total volume was the most sensitive to a wrong assumption of the refractive index, followed by the total surface area and then the total number of particles (left side of Table 3). The effective radius was always overestimated and, assuming a real refractive index when the true value was complex, it contributed to the enhancement of this overestimation. The average errors decreased when the real part of the assumed refractive indices was made smaller.

The propagation of the errors in the optical properties (left side of Table 3) was as follows. The average errors and standard deviations in the scattering coefficients were less than 0.2% when both the true and the assumed refractive indices were real. However, when the refractive indices had different imaginary parts, the average errors increased as a result of the different absorption. For example, the scattering coefficients reached average errors of 16% when real refractive indices were assumed in the inversion and the imaginary part of the true refractive index was -0.01. The hemispheric backscattering coefficients were underestimated or overestimated depending on whether the assumed real refractive index was larger or smaller than the true value, respectively. When the imaginary parts of the true and assumed refractive indices were different, the situation became more complicated. The errors in the hemispheric backscattering to total scattering ratio closely followed the errors in the hemispheric backscattering coefficients, except when any of the refractive indices were complex (Table 4). The asymmetry factor was not very sensitive to wrong assumptions of the refractive index (Table 5). Note that the errors in $g(\lambda, m')$ are much smaller than in $R(\lambda, m')$. This was expected as has been discussed in section 2c [see discussion of equations (16) and (18)]. The errors in the mass scattering efficiencies depended more on the errors in the retrieved total volume than on the effect of the wrong assumption of the refractive indices.

2) EFFECTS OF VARYING THE REFRACTIVE INDEX WITH PARTICLE SIZE

Usually, each mode of the size distribution has a different composition, that is, different refractive index. Gillespie et al. (1978) showed that the errors in the extinction coefficients when using an average value ($1.5-0.005i$) instead of separate refractive indices for each mode ($1.8-0.5i$ and $1.5-0i$ for the accumulation and coarse mode, respectively) were 15% at 0.55 μm and 2% at 1.06 μm. King et al. (1978) suggested that this effect would alter slightly the retrievals for particles with radius $0.1 \leq r \leq 1.0$ μm, while having little effect on particles with $r \geq 1.0$ μm. However, Gillespie et al. (1978) also demonstrated that the assumption of an average complex refractive index for the atmospheric aerosol may lead to significant differences in the results of the Mie calculations for the scattering, the absorption, and the hemispheric backscattering coefficients. To study how the retrieved parameters are affected when these discrepancies propagate to the inverted size distributions, we proceeded as follows.

1) Let the size distribution be $n(r)$. (We used size distribution D in Table 1 to focus on the different con-

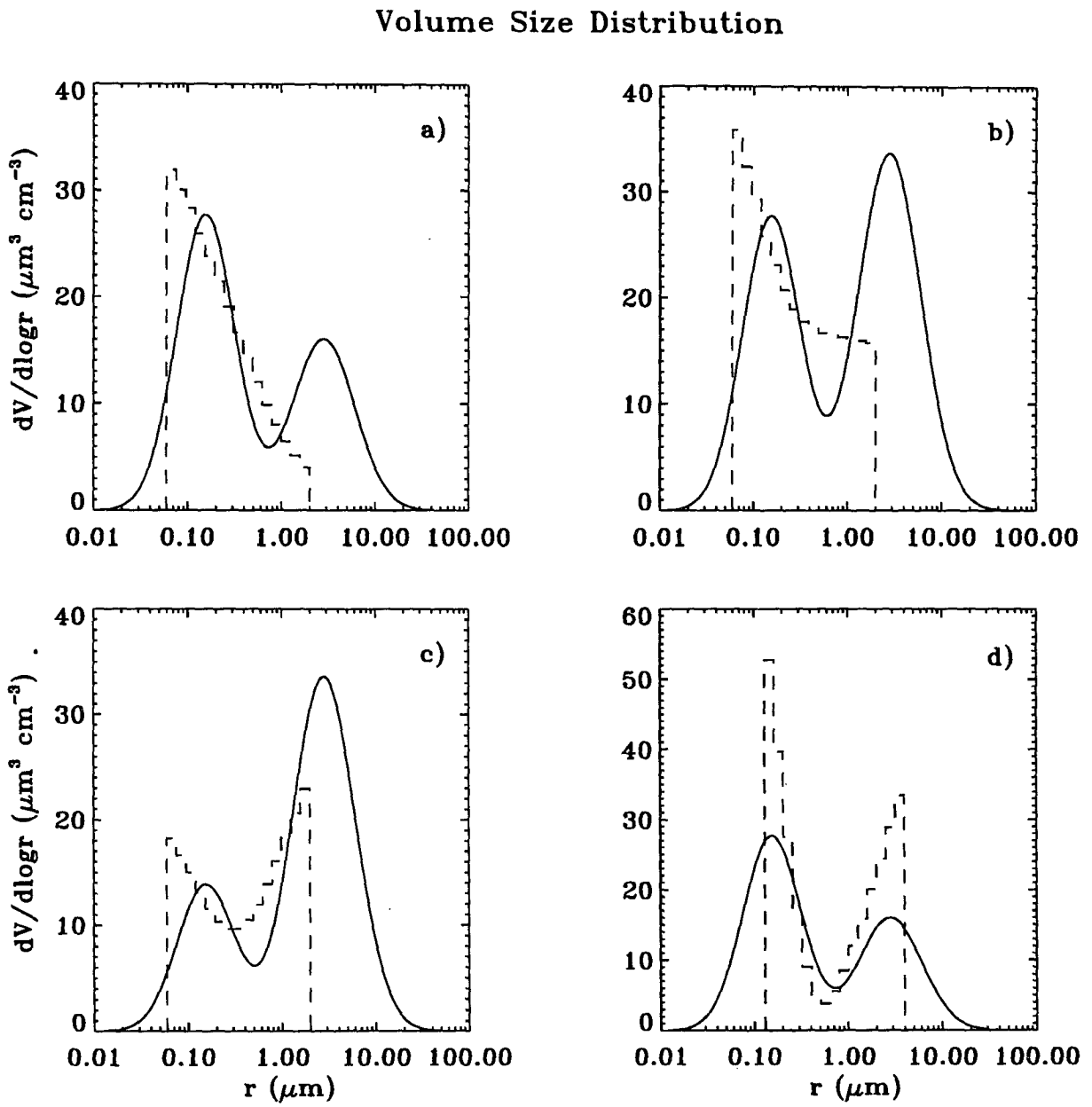

FIG. 4. Volume size distributions inferred from optical depths at 0.35-, 0.615-, and 0.88-μm wavelength (histograms). The refractive index was 1.40 throughout the process. The optical depths were generated for the following distributions (solid line, see Table 1). (a) Size distribution E: the retrievals show monomodal nature when the volume of the accumulation mode is greater than the volume of the coarse mode. (b) Size distribution D: the retrievals try to recover the coarse mode when both volumes are similar. (c) Size distribution F: the retrievals show bimodal nature when the volume of the accumulation mode is smaller than the volume of the coarse mode. (d) Size distribution E: even though the volume of the accumulation mode is greater than the volume of the coarse mode, the retrievals show bimodal nature. Note that in this case the radius interval is smaller and shifted to larger sizes.

tributions of each mode due only to its composition and not to its concentration.) Let m_a and m_c denote the refractive indices of the accumulation and the coarse modes, respectively.

2) Calculate $\tau(\lambda, m_a, m_c)$, $\sigma_{sp}(\lambda, m_a, m_c)$, $\sigma_{bsp}(\lambda, m_a, m_c)$, $\sigma_e(\lambda, m_a, m_c)$, N, S, V, r_{eff}, $R(\lambda, m_a, m_c)$, $g(\lambda, m_a, m_c)$, $\alpha_{sp}(\lambda, m_a, m_c)$.

3) Infer the size distribution $n'(r)$ from $\tau(\lambda, m_a, m_c)$ assuming the refractive index m' in the inversion algorithm.

4) Calculate $\sigma'_{sp}(\lambda, m')$, $\sigma'_{bsp}(\lambda, m')$, $\sigma'_e(\lambda, m')$, N', S', V', r'_{eff}, $R(\lambda, m')$, $g'(\lambda, m')$, $\alpha'_{sp}(\lambda, m')$ for $n'(r)$.

5) Compare Eqs. (2) and (4).

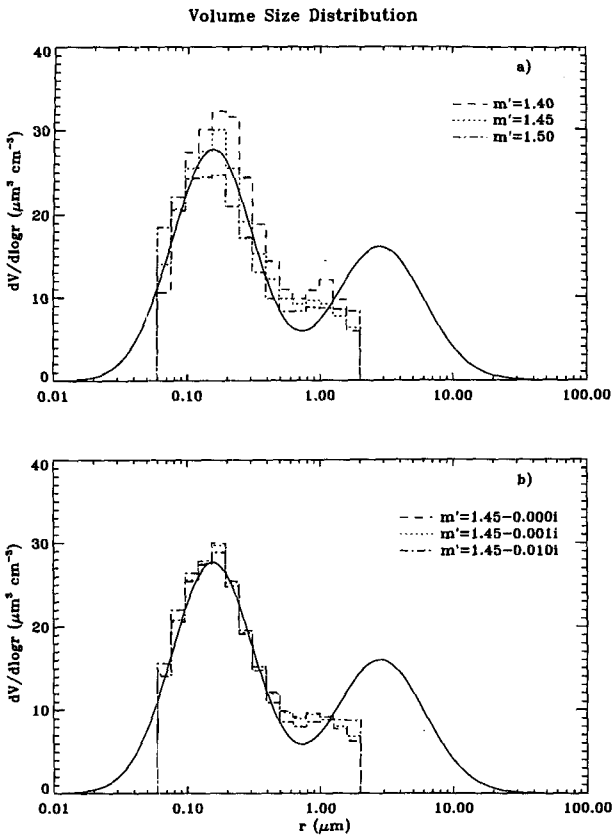

FIG. 5. Retrieved volume size distributions (histograms) for a variety of assumed refractive indices: (a) 1.40, 1.45, and 1.50 and (b) $1.45 + 0.0i$, $1.45 + 0.001i$, and $1.45 + 0.01i$. The optical depths were generated for the bimodal size distribution E (solid line, see Table 1) using the real refractive index 1.45.

6) Repeat for many different m'.
7) Repeat for many different m_a and m_c.

The results of this test were similar to the results of the previous section and are shown in the right side of Table 3. The retrieved scattering coefficients again were worse when one of the refractive indices was complex, but the average errors were always less than $\pm 10\%$. When m_a and m_b differed in their real parts, the hemispheric backscattering coefficients were best estimated when $m' = m_a$ was assumed in the inversion. This also applied to other optical parameters because the composition of the accumulation mode dominated in the inversion and the coarse mode seemed to play a minor role. Therefore, assuming in the inversion $m' = m_a$ led to the best calculated parameters. When m_a and m_b only differed in the imaginary parts, assuming m' equal to that of larger imaginary part yielded the best results. Also, the standard deviations of the average errors reached the lower values when m_a or m_b were complex. The asymmetry factor was much better retrieved than the hemispheric backscattering to total scattering ratio.

3) EFFECTS OF VARYING THE REFRACTIVE INDEX WITH WAVELENGTH

The wavelength dependence of the true refractive index has been ignored until now. We evaluated this approximation as follows.

1) Assume the size distribution $n(r)$ and the wavelength-dependent refractive index, $m = m(\lambda)$. We used the refractive indices of sulfuric acid solutions having concentrations by weight of 75% and 50%, as reported by Palmer and Williams (1975). These sulfuric acid solutions can be found in the atmosphere for relative humidity of approximately 35% and 60%, respectively (Charlson 1978). We also included the refractive indices of ammonium sulfate (crystals) reported by Toon et al. (1976). The refractive indices and their wavelength dependencies are shown in Table 6.
2) Calculate $\tau(\lambda, m)$, $\sigma_{sp}(\lambda, m)$, $\sigma_{bsp}(\lambda, m)$, $\sigma_e(\lambda, m)$, $N, S, V, r_{eff}, R(\lambda, m), g(\lambda, m), \alpha_{sp}(\lambda, m)$ for $n(r)$.
3) Retrieve the size distribution $n'(r)$ from $\tau(\lambda, m)$ assuming a constant refractive index m' corresponding to one of the wavelengths 0.35, 0.62, or 0.88 μm.
4) Calculate $\sigma'_{sp}(\lambda, m')$, $\sigma'_{bsp}(\lambda, m')$, $\sigma'_e(\lambda, m')$, $N', S', V', r'_{eff}, R'(\lambda, m'), g'(\lambda, m'), \alpha'_{sp}(\lambda, m')$ for the retrievals $n'(r)$.
5) Compare Eqs. (2) and (4).
6) Repeat for many different $n(r)$.

The most significant result was that the retrieved volume size distributions always had an extra mode in the accumulation size range (Fig. 6). The scattering and the hemispheric backscattering size distributions were also affected, showing this unrealistic mode in almost all the cases. The average errors in the moments of the size distribution were sometimes decreased by almost 30%. However, the standard deviations of the average errors were around 20%. The shapes of the retrievals were so distorted that a wide range of errors for N', S', and V' were found. The average errors in the effective radius were around -30% with standard deviations also around 20%.

In order to study the propagation of the uncertainties in the optical properties, the statistics for each true chemical composition of Table 6 were determined in two different ways: 1) calculating all the average errors for all the results including different wavelengths and 2) computing the average errors at each wavelength. The first way yielded approximately the same results as sections 3.2.1 and 3.2.2 except for the mass scattering efficiency. This retrieved parameter had much smaller average errors but for the wrong reason, as a result of the extra volume added to the retrievals. The second way yielded different behavior depending on the specific aerosol composition. The average errors in the hemispheric backscattering coefficient showed a strong wavelength dependence for several chemical components. The magnitude of these errors were directly reflected in the hemispheric backscattering to total scattering ratio. Table 7 shows that, for sulfuric acid

TABLE 3. Sensitivity to uncertainty in the refractive index. The two numbers for each entry are the minimum and maximum values obtained for different combinations of true and assumed refractive indices.[a]

Retrieved parameters	The true refractive index is the same for both accumulation and coarse modes[b]		The true refractive index is the combination of the true refractive indices m_a and m_c[c]	
	Average error (%)	Standard deviation	Average error (%)	Standard deviation
Total number	(−83, −80)	(5, 7)	(−79, −77)	(4, 5)
Total surface	(−37, −21)	(13, 17)	(−27, −15)	(5, 6)
Total volume	(−44, −24)	(13, 24)	(−38, −26)	(4, 8)
Effective radius	(−9, 2)	(20, 41)	(−18, −12)	(0.2, 3)
Total scattering coefficient	(−12, 16)	(1, 6)	(−9, 6)	(1, 3)
Hemispheric backscattering coefficient	(−20, 48)	(6, 24)	(−21, 24)	(3, 7)
Hemispheric backscattering to total scattering ratio	(−20, 29)	(6, 14)	(−21, 17)	(3, 7)
Asymmetry factor	(−9, 7)	(1, 4)	(−6, 7)	(0.5, 2)
Mass scattering efficiency	(33, 108)	(38, 75)	(30, 70)[‡]	(6, 17)
	All bimodal size distributions of Table 1 are considered		Only size distribution D of Table 1 is considered	

[a] The average errors and the standard deviations were calculated as in Table 2. The statistics were performed separately for each case of true (m) and assumed (m') refractive indices and included all the inversion results.

[b] The combinations of m and m' are as in Tables 4 and 5, and the number of retrievals varies between 126 and 177.

[c] The combinations of the true refractive indices of the accumulation (m_a) and the coarse (m_c) modes are (m_a, m_c) = [(1.45, 1.50); (1.45, 1.45 + 0.001); (1.45, 1.45 + 0.01); (1.50, 1.45); (1.50, 1.45 + 0.01); (1.45 + 0.01, 1.45); (1.45 + 0.01, 1.50)]. The m' are as in Tables 4 and 5. The number of retrievals varies between 126 and 177.

at 50% concentration, the average errors in R' reached values larger than 30% at the shorter wavelengths, while the average errors in the asymmetry factor stayed under 8%. Similar results were obtained for sulfuric acid at 75% concentration (not shown). For ammonium sulfate, average errors in both R' and g' were smaller than 10%.

An explanation of why the inversion program returns these solutions can be found from the extinction size distributions for sulfuric acid at 50% concentration (Fig. 7). They are shifted not just in radius at the different wavelengths, but also in magnitude for the different refractive indices. The three curves in Fig. 7a approximately agree in magnitude except in the interval of sizes 0.1–0.4 μm. When the refractive indices 1.396 or 1.392 were assumed in the inversion, the retrievals needed to have more particles in this range in order to reproduce the scattering coefficients computed for the refractive index 1.43 at the shorter wavelengths. On the other hand, at larger wavelengths (Fig. 7b) the retrievals had to decrease the number of particles in this size range to avoid overestimating the extinction coefficient. Therefore, the algorithm decided to exclude these sizes and make use of the particles smaller than 0.1 μm, taking advantage of the decreasing efficiency factors with wavelength. This introduces dramatic errors in the other optical properties, especially in those with efficiency factors with shapes not similar to the extinction efficiency, such as the hemispheric backscattering coefficients. However, the extinction size distributions for ammonium sulfate (not shown) were very little shifted

TABLE 4. Average errors in the retrieved hemispheric backscattering to total scattering ratio. The standard deviations are between 6% and 14%. The statistic includes all the results of the inversion for the optical depth generated for all the bimodal-size distributions of Table 1. The average errors and the standard deviations of the errors have been calculated as in Table 2.

R' True refractive indices	Refractive indices assumed in the inversion				
	1.40	1.45	1.50	1.45 + 0.001i	1.45 + 0.01i
1.40	1	15	29	14	4
1.45	−10	2	14	1	−7
1.50	−20	−8	4	−10	−16
1.45 + 0.001i	−8	4	17	3	−5
1.45 + 0.01i	−1	13	27	12	3

TABLE 5. Average errors in the retrieved asymmetry factor (the standard deviations are between 1% and 4%), as in Table 4.

g' True refractive indices	Refractive indices assumed in the inversion				
	1.40	1.45	1.50	1.45 + 0.001i	1.45 + 0.01i
1.40	−1	−5	−9	−5	−2
1.45	3	−1	−5	−1	1
1.50	7	3	−2	3	5
1.45 + 0.001i	2	−2	−6	−1	1
1.45 + 0.01i	0.5	−4	−8	−3	−1

TABLE 6. Refractive indices used to generate the input optical depths (Palmer and Williams 1975; Toon et al. 1976).

Wavelength	Sulfuric acid 50%	Sulfuric acid 75%	Ammonium sulfate
0.35	1.430	1.460	1.540
0.44	1.403	1.433	1.535
0.53	1.398	1.431	1.530
0.62	1.396	1.430	1.527
0.70	1.394	1.428	1.525
0.79	1.393	1.427	1.520
0.88	1.392	1.425	1.518

for different refractive indices, and the retrieved size distribution for this chemical component was much less distorted with smaller errors (Table 7).

4) EFFECTS OF MIXING NONABSORBING WITH STRONGLY ABSORBING AEROSOLS IN THE ACCUMULATION MODE

Very often, especially in polluted areas, light-absorbing carbon particles coexist with nonabsorbing aerosol particles. The particles can be *externally mixed,* where individual particles contain only one chemical species, or *internally mixed,* where an individual particle contains multiple chemical species. The different species can be distributed homogeneously throughout the internally mixed particles, or they can consist of one or more insoluble cores coated with a soluble shell. Moreover, the particles may not be symmetric and minor components can be located anywhere inside a major component.

In sections 3b(1) and 3b(2), the true optical properties of absorbing particles were calculated assuming a homogeneous, internal mixture of absorbing and nonabsorbing species, and the retrievals assumed either nonabsorbing particles or homogeneous, internal mixtures. This section studies how a lack of knowledge of the aerosol state of mixing propagates to the retrieved parameters for the case where the particles are externally mixed. The simplified model consists of the following assumptions.

1) Strongly absorbing particles (e.g., carbonaceous soot) are represented by a refractive index $1.8-0.5i$ (see Gillespie et al. 1978). The nonabsorbing component is represented by a refractive index 1.40, typical of sulfuric acid at visible light for 60% relative humidity (see Table 6). The calculations are made for volume percentages of the light-absorbing components of 5% and 0.5%. These refractive indices and volume percentages yield single scattering albedos varying from 0.7 to 0.9, roughly spanning the range of observations reported by Waggoner et al. (1981).

2) The externally mixed and internally mixed particles are assumed to have the same size distribution described by the accumulation modes of Table 1 (size distributions A, B, and C). The effects of uncertainties in size distribution were studied in section 3b(2).

We proceeded as follows.

1) Calculate the optical properties of the absorbing and nonabsorbing components separately for the size distributions A, B, C, as in section 3a. Then calculate the optical properties of the mixture as the volume-weighted average of the two components.

2) Infer $n'(r)$ from the optical depths calculated in Eq. (1) as in section 3a, assuming refractive indices m' of 1.40 and $1.42-0.025i$. The latter value is the volume-weighted refractive index of the two components, $(0.95*1.40 + 0.05*1.8) - (0.95*0.0 + 0.05*0.5)i$ and represents the refractive index of the volume mixed particles (Ackerman and Toon 1981).

3) Calculate $\sigma'_{sp}(\lambda, m')$, $\sigma'_{bsp}(\lambda, m')$, $\sigma'_e(\lambda, m')$, $N', S', V', r'_{eff}, R'(\lambda, m'), g'(\lambda, m'), \alpha'_{sp}(\lambda, m')$ for the retrievals, $n'(r)$.

4) Compare Eqs. (1) and (3).

5) Again, infer $n'(r)$ but now from the optical depth of the nonabsorbing particles, assuming the refractive index m' of $1.42-0.025i$ and also kernels for an external mixture. In the kernels for an external mixture, the Mie extinction efficiency factors are obtained as the volume-weighted average of the Mie extinction efficiency factors of the two components.

6) Calculate the optical properties for the retrievals, $n'(r)$, for both internal and external mixtures.

7) Compare the optical properties of the nonabsorbing component calculated in (1) and the optical properties calculated in (6).

8) Repeat for 0.5% volume fraction of light absorbing particles.

The results are summarized in Table 8 and are similar to the results of sections 3b(1) and 3b(2). The

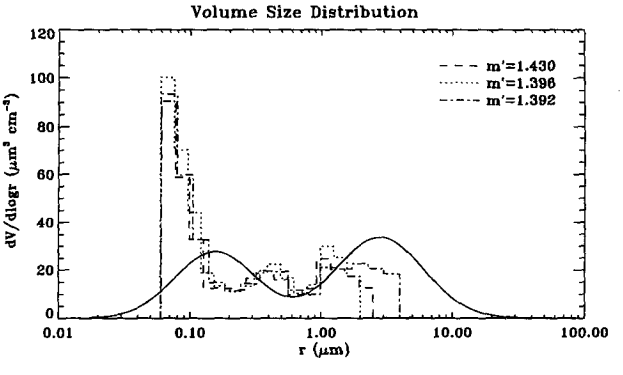

FIG. 6. Retrieved volume size distributions assuming the refractive indices 1.43, 1.396, and 1.392. The optical depth data were generated for the bimodal size distribution D (solid line, see Table 1) using the wavelength-dependent refractive index for a sulfuric acid solution having 50% concentration by weight (see Table 4). The accumulation mode is divided into two modes and the minimum between them is approximately located between 0.1 and 0.4 μm.

TABLE 7. Average errors and standard deviations in the hemispheric backscattering to total scattering ratio and the asymmetry factor. The statistics were performed as in Table 2 including all the results for m' (refractive indices at 0.35, 0.62, 0.88 μm of Table 6). The input optical depths were generated for all the bimodal distributions in Table 1 using the wavelength-dependent refractive indices of Table 6.

	Sulfuric acid 50%				Ammonium sulfate			
	R		g		R		g	
Wavelength (μm)	Average error (%)	Standard deviation	Average error (%)	Standard deviation	Average error (%)	Standard deviation	Average error (%)	Standard deviation
0.35	10	20	−4	4	−6	9	0.7	2
0.44	31	21	−8	4	−4	10	0.4	3
0.53	30	17	−7	3	−1	9	−0.3	3
0.62	23	12	−5	2	5	9	−2	3
0.70	19	8	−4	2	6	10	−2	3
0.79	12	6	−3	2	7	9	−3	3
0.88	8	6	−2	2	6	10	−2	4

errors in the retrieved moments of the size distributions are systematically large, and the asymmetry factor is always the best retrieved parameter with the smallest standard deviation of the average error. The retrieved parameters for 0.5% volume fraction of absorbing particles are not shown in Table 8 because they have smaller errors than the retrieved parameters for 5% volume fraction of absorbing particles. For externally mixed aerosols, the retrieved asymmetry factors are obtained with little errors assuming either the sulfuric acid refractive index, or the volume-weighted refractive index of the absorbing and nonabsorbing components. Similar results are obtained when assuming external mixture or internal mixture in the inversion of nonabsorbing particle optical depths. For all the cases studied, the asymmetry factor is obtained with an error less than 5%, which suggests that the asymmetry factor is relatively insensitive to the state of mixture.

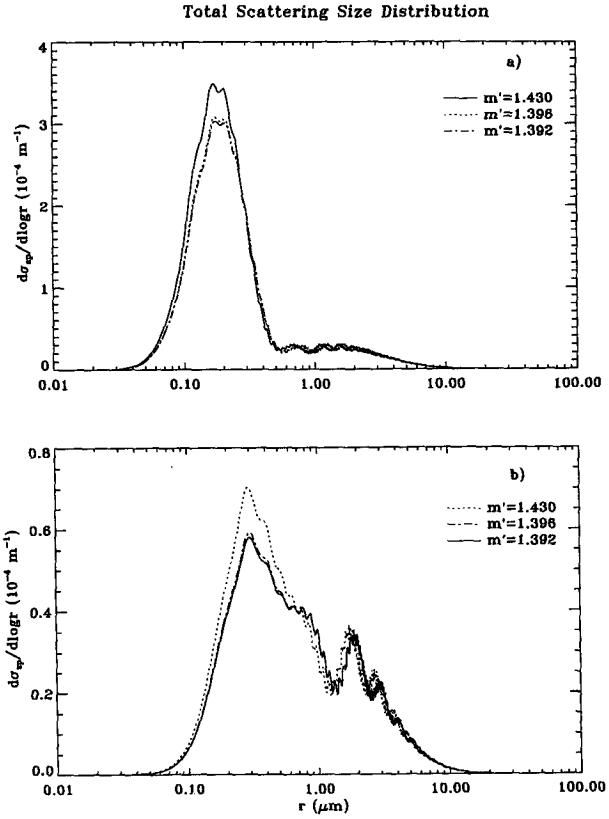

FIG. 7. Scattering size distributions generated for the bimodal size distribution F (see Table 1) using the refractive indices 1.43, 1.396, and 1.392 at the wavelengths (a) 0.35 and (b) 0.88 μm. The differences between the three curves are in the radius interval from 0.1 to 0.4 μm. The extra minimum of the retrievals of Fig. 5 is approximately located in the same interval.

Ackerman and Toon (1981) computed the Mie scattering phase function assuming 10% soot and 90% sulfate for shell-coated particles, external and volume states of mixing, and pure sulfate particles. They showed that 1) the phase function is the same for external mixtures and for pure sulfate particles; 2) the aerosol phase functions for shell-coated particles and volume mixtures are equal to the sulfate aerosol phase function in the forward direction but they differ in the backward direction; 3) the phase functions in the backward direction differ for shell-coated particles and volume mixtures phase function, but not as much as they both differ from the sulfate particle phase function; and 4) the largest differences are at a scattering angle of 180° and do not change substantially for soot volume percentages varying from 5% to 80%. Therefore, since the retrieved asymmetry factor is weakly sensitive to state of mixing, it may be expected that this parameter will be retrieved with small errors for shell-coated particles, assuming the volume-weighted refractive index.

Chylek et al. (1995) have also studied the optical properties of sulfate aerosols that contain black carbon. They concluded that, independently of where the carbon is located inside the particle, the extinction coefficient and the asymmetry factor can be calculated to a good approximation considering sulfate spheres. Then,

TABLE 8. Sensitivity to a lack of knowledge of the state of mixing for 5% and 95% volume fractions of absorbing and nonabsorbing particles, respectively.

Retrieved parameters	External mixture of absorbing and nonabsorbing particles				Nonabsorbing homogeneous particles			
	Average error (%)	Standard deviation	Average error (%)	Standard deviation	Average error (%)	Standard deviation	Average error (%)	Standard deviation
	True state of mixing[a]							
Total number	−87	5	−84	5	−79	3	−71	7
Total surface	−34	8	−30	5	−24	3	−18	6
Total volume	−4	5	−10	3	−12	2	−12	2
Effective radius	47	12	29	6	16	3	7	5
Total scattering coefficient	10	4	−9	1	−9	3	−2	5
Hemispherical backscattering to total scattering ratio	−11	7	−3	9	10	9	−2	10
Asymmetry factor	3	1	−0.3	5	−4	4	−0.4	3
Mass scattering efficiency	15	12	2	19	4	36	11	16
	Assumed state of mixing[b]							
	Nonabsorbing homogeneous particles		Homogeneous, internal mixture of absorbing and nonabsorbing particles		External mixture of absorbing and nonabsorbing particles		Homogeneous, internal mixture of absorbing and nonabsorbing particles	

[a] The true optical properties for homogeneous, nonabsorbing particles have been calculated for a refractive index of 1.40. The true optical properties for homogeneous, absorbing particles have been calculated for a refractive index of $1.8-0.5i$. The true optical properties for externally mixed particles have been calculated as the volume-weighted averages of the optical properties of the absorbing and nonabsorbing particles.

[b] The nonabsorbing particles are represented by a refractive index of 1.40. The strongly absorbing particles are represented by a refractive index of $1.8-0.5i$. The homogeneously, internally mixed particles are represented by the refractive index of $1.42-0.025i$, obtained as the volume weighted average refractive index of the two components, $(0.95*1.40 + 0.05*1.8) - 0.05*0.5i$. The externally mixed particles cannot be represented by a unique refractive index, and the extinction efficiency factors are obtained as the volume-weighted average efficiency factors of the two components, $0.95*Q_e(r, m_{\text{nonabsorbing}}, \lambda) + 0.05*Q_e(r, m_{\text{absorbing}}, \lambda)$.

since the uncertainties in the location of the carbon component within the sulfate particle do not affect the extinction coefficient (input data to the inversion program) or the true asymmetry factor, we would expect to retrieve asymmetry factors with little sensitivity for these inhomogeneous, internally mixed particles.

4. Conclusions

Optical depth spectra were generated for monomodal and bimodal size distributions using Mie theory. The inversion algorithm of King et al. (1978) was used to retrieve the original size distribution from the optical depths. Then the moments and the optical properties calculated for the retrievals were compared with their true values. First the composition was assumed to be known and the refractive index of the particles stayed constant throughout the process. Second, the errors resulting from the uncertainties in the refractive index of the particles were studied in different ways: 1) assumed refractive index constant for all particle sizes and wavelengths; 2) assumed refractive index constant for all wavelengths but different for accumulation and coarse mode particles; and 3) refractive index constant for all particle sizes but with a dependence on wavelength.

The large errors in the moments of the size distributions (total number of particles, total surface, and total volume) are related to the lack of information given to the inversion algorithm. Therefore, complementary information about the less optically efficient sizes at visible wavelengths is necessary to reproduce the true moments as well as the true shapes of the size distributions. Independent information about the coarse mode is also desirable. Otherwise, the effective radius and any other magnitude defined by the ratio of an optical property and a moment of the size distribution is prone to substantial error. The additional information can be of any kind, for example, inverting hemispherical backscattering coefficients, total scattering coefficients, and particle number concentrations in different size ranges simultaneously (Heintzenberg 1980).

Uncertainty in the real part of the aerosol refractive index leads to larger errors in the hemispheric backscattering to total scattering ratio, R, than in the asymmetry factor, g. For example, when the difference between the real parts of the assumed and the true refractive indices is 0.1, the average errors are 26% and 9% in R and g, respectively. However, there is little sensitivity to the imaginary part of the refractive index. Also, g is one of the least variable retrieved parameters for the many inversion solutions.

When the true wavelength dependence of the refractive index is considered, the retrievals yield an unreal-

istic minimum in the volume distribution from 0.1 to 0.4 μm radius. This distortion of the size distribution is caused by the magnitude shifts of the extinction size distribution for the true and assumed refractive indices. When the refractive indices for two successive wavelengths are quite different, the assumption of a constant value in the inversion can lead to average errors around 30% in both the hemispheric backscattering coefficients and the hemispheric backscattering to total scattering ratio. However, the magnitude of the average errors in the asymmetry factor stays under 8%. Any inversion code that retrieves size distributions from multiwavelength optical depths without assuming the refractive index dependency on wavelength will be prone to these errors.

Inversion algorithms are subject to many systematic errors such as finite size range of the retrieval, uncertainties in the refractive index, and finite set of input wavelengths, which depend on the actual size distribution. The errors in the retrieved parameters depend also on the efficiency factors that define the input data. Moreover, some aerosol properties that have large errors when they are obtained from spectral optical depths may be retrieved better from other set of input data. Therefore, extra caution must be taken when using inversion results to derive aerosol properties or when interpreting the retrieved size distributions. In this regard, it is useful to perform a sensitivity study simulating the actual experimental conditions of each measurement and the inversion process.

Even though the retrievals may not reproduce the actual size distribution, those integral optical properties with kernel function similar to the efficiency factors of the input data will be retrieved with much less dependence on the inversion assumptions. Furthermore, the retrieved size distributions can be used as an intermediate step for extrapolating one set of optical properties to another set of optical properties. In particular, the asymmetry factor can be retrieved from spectral optical depth data with little sensitivity to the assumptions in the inversion.

Acknowledgments. The authors are grateful to B. Stone and E. Dutton for helpful discussions on both the inversion and Mie algorithms. Comments on the original version of the manuscript by B. Stone are also acknowledged. This work was performed while HGJ was a visiting scientist at CMDL and she thanks the staff of CMDL for their hospitality.

REFERENCES

Ackerman, T. P., and O. B. Toon, 1981: Absorption of visible radiation in atmosphere containing mixtures of absorbing and nonabsorbing particles. *Appl. Opt.*, **20,** 3661–3668.

Charlson, R. J., 1978: Chemical properties of tropospheric sulfur aerosols. *Atmos. Environ.*, **12,** 39–53.

——, J. Lagner, H. Rodhe, C. B. Leovy, and S. G. Warren, 1991: Perturbation of the Northern Hemisphere radiative balance by backscattering from anthropogenic sulfate aerosols. *Tellus,* **43AB,** 152–163.

——, S. E. Schwartz, J. M. Hales, R. D. Cess, J. A. Coakley Jr., J. E. Hansen, and D. J. Hofmann, 1992: Climate forcing by anthropogenic aerosols. *Science,* **255,** 423–430.

Chylek, P., G. Videen, D. Ngo, R. G. Pinnick, and J. D. Klett, 1995: Effect of black carbon on the optical properties and climate forcing of sulfate aerosols. *J. Geophys. Res.,* **100**(D8), 16 325–16 332.

Dellago, C., and H. Horvarth, 1993: On the accuracy of the size distribution information obtained from light extinction and scattering measurements—I. Basic considerations and models. *J. Aerosol Sci.,* **24,** 129–141.

Gillespie, J. B., S. G. Jennings, and J. D. Lindberg, 1978: Use of an average refractive index in atmospheric propagation calculations. *Appl. Opt.,* **17,** 989–991.

Grassal, H., 1971: Determination of aerosol size distributions from spectral attenuation measurements. *Appl. Opt.,* **10,** 2534–2538.

Hansen, J. E., and A. A. Lacis, 1990: Sun and dust versus greenhouse gases: An assessment of their relative roles in global climate change. *Nature,* **346,** 713–719.

Heintzenberg, J., 1975: Determination in situ of the size distribution of the atmospheric aerosol. *J. Aerosol Sci.,* **6,** 291–303.

——, 1978: Particle size distributions from scattering measurements of non-spherical particles via Mie-theory. *Beitr. Phys. Atmos.,* **51,** 91–99.

——, 1980: Particle size distributions and optical properties of Arctic haze. *Tellus,* **32,** 251–260.

——, H. Müller, H. Quenzel, and E. Thomalla, 1981: Information content of optical data with respect to aerosol properties: Numerical studies with a randomized minimization-search-technique inversion algorithm. *Appl. Opt.,* **20,** 1308–1315.

Kiehl, J. T., and B. P. Briegleb, 1993: The relative role of sulfate aerosols and greenhouse gases in climate forcing. *Science,* **260,** 311–314.

King, M. D., 1982: Sensitivity of constrained linear inversions to the selection of the Lagrange multiplier. *J. Atmos. Sci.,* **39,** 1356–1369.

——, D. M. Byrne, B. M. Herman, and J. A. Reagan, 1978: Aerosol size distributions obtained by inversion of spectral optical depth measurements. *J. Atmos. Sci.,* **35,** 2153–2167.

Nakajima, T., M. Tanaka, and T. Yamauchi, 1983: Retrieval of the optical properties of aerosols from aureole and extinction data. *Appl. Opt.,* **22,** 2951–2959.

Palmer, K. F., and D. Williams, 1975: Optical constants of sulfuric acid; application to the clouds of Venus. *Appl. Opt.,* **14,** 208–219.

Schneider, S. H., 1994: Detecting climatic change signals: Are there any "fingerprints"? *Science,* **263,** 341–346.

Shaw, G. E., 1979: Inversion of optical scattering and spectral extinction measurements to recover aerosol size spectra. *Appl. Opt.,* **18,** 988–993.

Tang, I. N., and H. R. Munkelwitz, 1994: Water activities, densities, and refractive indices of aqueous sulfates and sodium nitrates droplets of atmospheric importance. *J. Geophys. Res.,* **99,** 18 801–18 808.

Taylor, K. E., and J. E. Penner, 1994: Response of the climate system to atmospheric aerosols and greenhouse gases. *Nature,* **369,** 734–737.

Toon, O. B., J. B. Pollack, and B. N. Khare, 1976: The optical constants of several atmospheric aerosol species: Ammonium sulfate, aluminum oxide and sodium chloride. *J. Geophys. Res.,* **81,** 5733–5748.

Twomey, S., 1977: *Introduction to the Mathematics of Inversion in Remote Sensing and Indirect Measurements.* Elsevier, 243 pp.

Waggoner, A. P., R. E. Weiss, N. C. Ahlquist, D. S. Covert, S. Will, and R. Charlson, 1981: Optical characteristics of atmospheric aerosols. *Atmos. Environ.,* **15,** 1891–1909.

Whitby, K. T., 1978: The physical characteristics of sulfur aerosols. *Atmos. Environ.,* **12,** 135–159.

Wiscombe, W. J., 1980: Improved Mie scattering algorithms. *Appl. Opt.,* **19,** 1505–1509.

Yamamoto, G., and M. Tanaka, 1969: Determination of aerosol size distribution from spectral attenuation measurements. *Appl. Opt.,* **8,** 447–453.